J Electroceram (2009) 23:103–109
DOI 10.1007/s10832-007-9316-y

Analytical estimation of high-frequency properties of RF micro-inductors prepared by direct-write techniques

Eui-Jung Yun · Jae-Wook Kim · Won-Gook Lee · Young-Jin Kim · Hyeong-Sik Park

Received: 16 May 2007 / Accepted: 16 August 2007 / Published online: 22 September 2007

Abstract In this work, the high-frequency characteristics of micron size, square spiral-type RF thin film air-core inductors prepared by direct-write supersonic jet deposition of laser ablated nanoparticle were estimated by a software package. The important parameters that are determined by direct-write process, such as the materials, the cross-section shape, the thickness, and the conductivity of the coil, were varied systematically to estimate the trend of the inductors' performances. The area dimensions of RF inductors utilized and the number of coil turns were 1.3 mm × 1.3 mm and 3, respectively. The 96 wt% Al_2O_3, SiO_2-coated Al_2O_3, and SiO_2-coated Si wafers were used as the substrate material. The high-frequency characteristics of the inductance (L) and quality factor (Q) of the utilized inductors were simulated using a Maxwell three-dimensional field simulator (HFSS 8.5), which employs the finite element method. The used inductors, which have silver metal (Ag) coils, the trapezoid shaped cross-section of the coil, the coil thickness of 30 μm, and the coil conductivity of 70% of Ag bulk value, exhibit L of 8 to 9 nH. They also exhibit a maximum Q of 35.5 near the frequency of 750 MHz and a self-resonant frequency of 5.14 GHz. The simulated high-frequency data of the inductors were agreed well with those obtained from the equivalent circuit model of the utilized inductors.

Keywords RF micro-inductors · Square spiral-type · Direct-write process · High-frequency structure simulator

1 Introduction

Silicon-based radio frequency (RF) integrated inductors are one of the essential passive components in the circuitry of the latest electronic products, [1–9] e.g., in notebook computers, camcorders, pagers, cellular phones, and etc. One major application of planar inductors includes operation in very-high-frequency regimes (>GHz) as inductive components in microwave circuits as well as in signal processing circuits.

In recent years, researchers have realized various high-quality factor (Q) and self-resonant frequency (SRF) three-dimensional (3D) inductors using the complicated microelectromechanical systems (MEMS) technique [10–14]. Microinductors fabricated using MEMS techniques have Q of 6 to 55 at 1 GHz and L of 1.17 to 1.88 nH, and exhibit SRF of 2 to 10 GHz. These MEMS inductors sustain, however, severe performance degradation and even failure due to breaking of insulator at application temperature above 300°C, such as polyimide, etc. It was known that Al_2O_3 material has superiority for high temperature application because of its high melting point, high resistivity, high hardness, and vitreous transparence [12].

On the other hand, the direct-write techniques are being actively considered to simplify the fabrication processes of micro-inductors and can produce complex, micron scale devices in a relatively short period of time with less human

E.-J. Yun · H.-S. Park
Department of Semiconductor & Display Engineering,
Hoseo University,
Chungnam 336-795, South Korea

E.-J. Yun (✉) · W.-G. Lee · Y.-J. Kim
Department of Information & Control Engineering,
Hoseo University,
Chungnam 336-795, South Korea
e-mail: ejyun@office.hoseo.ac.kr

J.-W. Kim
Department of Electronics Engineering, Namseoul University,
Chungnam 330-707, South Korea

participation and intermediate processing steps by eliminating many processing steps required by traditional techniques such as lithography and etch etc [15, 16]. In general any materials in the form of fine powder can be directly written into micro-inductor pattern with various techniques that include supersonic jet deposition of laser ablated nanoparticle (NP), micropen, ink jet, and focused ion beam etc. It has been demonstrated that the method of supersonic jet deposition of laser ablated NP is to be an excellent technique for micron scale components [17] in the sense that: (1) it provides significant environmental benefits by eliminating the waste associated with traditional processes and (2) it can deposit a wide variety of materials, such as metals, semiconductors, and insulators, on any surfaces—silicon, glass, plastics, metals, ceramics, and polymers—at both high- and low-temperature substrates.

From this viewpoint, in this study, the high-frequency characteristics of simple, micron size, square spiral-type RF thin film air-core inductors prepared by direct-write supersonic jet deposition of laser ablated silver NP were estimated by a software package [a high-frequency structure simulator (HFSS) 8.5)]. The substrate material of 96 wt% Al_2O_3 selected by the reason mentioned above was used for the simulation.

2 Simulation of micron size RF inductors realized by direct-write process

The important parameters that are determined by direct-write process, such as the materials, the cross-section shape, the thickness, and the conductivity of the coil, were varied systematically to estimate the trend of the inductors' performances. Figure 1 shows the structure of the typical RF micro-inductors employed for the computer simulation. The area dimensions of RF inductors utilized and the number of coil turns were 1.3 mm×1.3 mm and 3, respectively. Either 96 wt% Al_2O_3 ceramic materials or SiO_2-coated Si wafers were used as the substrate material. Due to the skin effect of the internal conductor of coils in RFs, highly conductive silver metals, Ag, with the thickness ranges of 3 to 30 μm were used as the coils in order to decrease the metal loss of the micro-inductors. As shown in Fig. 1 the trapezoid shaped cross-section of the coil was considered specially here because that shape is usual in the cross-section of Ag lines prepared by direct-write supersonic jet deposition of laser ablated NP [18].

High-frequency characteristics of L and Q of the developed inductors were obtained from computer simulations. Simulations of the RF inductors are performed by using a software package [a high-frequency structure simulator (HFSS) 8.5)]. HFSS utilizes a 3D finite element method (FEM) to compute the electrical behavior of high-frequency components. The driven terminal method that employes more than two input signals and calculates the terminal-based S-parameters of passive, high-frequency structures with multi-conductor transmission line ports, which are driven by a source, was selected for the solution type. The lumped port was used. The virtual perfect E boundary with a rectangular shape was used to make a ground connection between two ports. The simulation conditions employed in this paper are as followes: (1) in analysis setup, solution frequency, maximum number of pass, and delta S were 12 GHz, 12, and 0.02, repectively, (2) the interpolating method was selected for sweep type, and (3) the frequency was varied from 0.01 to 10 GHz with increment of 0.01 GHz. The meshes are generated by an adaptive mesh generation method. The computer simulation is carried out until the total error rate is less than 2%.

The calculated data obtained from the equivalent circuit analysis of the developed RF inductors were compared with those obtained from computer simulations to confirm their high-frequency characteristics.

3 Results and discussion

First, the computer simulation was performed using various structures of the RF micro-inductor such as copper (Cu)/SiO_2/Si, Ag/SiO_2/Al_2O_3, and Ag/Al_2O_3 under the conditions as the coil thickness (t) of 3 μm and the rectangular shaped cross-section of the coil [a=0 μm, b=100 μm; see Fig. 1(b)]. The Cu/SiO_2/Si structure was employed because it is the typical structure of Si-based RF micro-inductors. The Ag/SiO_2/Al_2O_3 and Ag/Al_2O_3 structures were also considered mainly because of their simpler structure that can be adopted in RF micro-inductors prepared by direct-write techniques [18]. Figure 2 shows the variations of inductance-frequency (L-f) characteristics with three structures obtained from the computer simulation. As shown in Fig. 2, the L values are nearly constant at 8 nH up to 1 GHz and are slightly larger for Ag/SiO_2/Al_2O_3 and Ag/Al_2O_3 structures, indicating that the best structure will be the simple Ag/Al_2O_3 structure. Figure 3 also shows the variations of quality factor-frequency (Q-f) characteristics with three structures obtained from the computer simulation, illustrating that the highest maximum Q (Q_{max}) value of 38 at 700 MHz is observed for the structure of Ag/Al_2O_3. The self-resonant frequencies ($SRFs$) that are defined as the frequency where the falloff of L occurs in Fig. 2 and as the frequency where the Q value becomes zero in Fig. 3 are slightly larger (5.2 GHz) for Ag/Al_2O_3 structure. Thus, the Ag/Al_2O_3 structure was selected as the main structure for simulation mainly because of its simpler structure with the best Q_{max} among all considered structures suggested from the simulation results in Figs. 2 and 3.

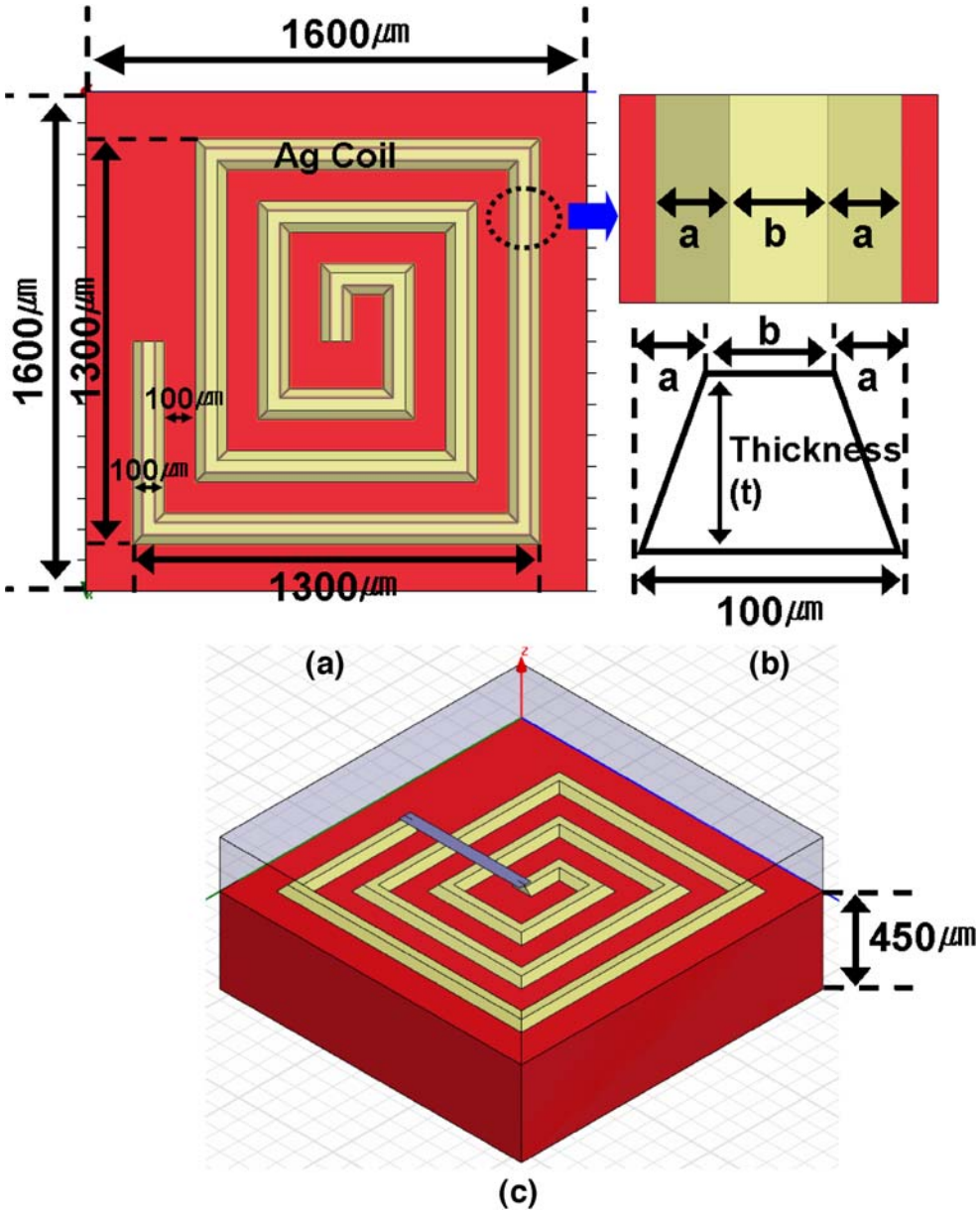

Fig. 1 Structure of the typical RF micro-inductors employed for the computer simulation: (**a**) top view, (**b**) cross-sectional view of the Ag coil, and (**c**) side view. The trapezoid shaped cross-section of the Ag coil was considered

Second, the computer simulation was performed using various shaped cross-sections of the coils and coil thicknesses under the same Ag/Al_2O_3 structure condition. Figure 4 shows the simulated *L-f* characteristics obtained from four different inductors with the combination of two coil thicknesses (t=3 and 30 μm) and two shapes of cross-section of the coils (rectangle with a=0 and b=100 μm and trapezoid with a=20 μm and b=60 μm). Here, we emphasize that the trapezoid shaped cross-section of the coils was considered mainly because of its usual shape in the cross-section of Ag lines prepared by direct-write techniques [18]. It was observed from Fig. 4 that the L values for the inductors with the trapezoid shaped cross-section of the coils (t=3 μm) are nearly constant at 8.6 nH up to 1 GHz while those with the rectangular shaped cross-section of the coils (t=30 μm) nearly constant at 7.3 nH in the frequency range 0.2–1 GHz, suggesting that the larger cross-sectional areas of the coil show the smaller L values. Figure 5 shows the simulated *Q-f* characteristics obtained from the same samples in Fig. 4, indicating that the highest Q_{max} value of 41 at 700 MHz is observed for the inductors with t=30 μm and trapezoid shaped cross-section of the coils (a=20 μm and b=60 μm). The larger cross-sectional areas of the coil, thus smaller resistance of the coil resulted in the larger Q effects during high-frequency operation. It was concluded from Fig. 5 that the desired Q_{max} can be achieved by optimizing t, a, and b values. The *SRFs* are also constant at 5.2 GHz for all samples as shown in Figs. 4 and 5.

Third, the computer simulation was performed using various a and b values in trapezoid shaped cross-section of

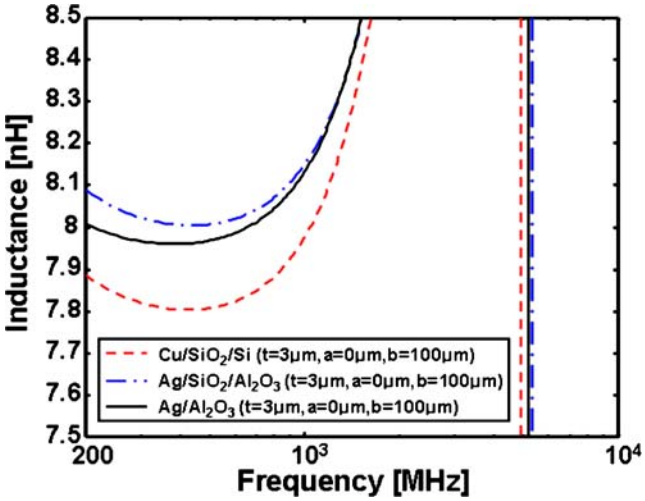

Fig. 2 Simulation results of the *L-f* characteristics with three structures obtained under the conditions as the coil thickness (t) of 3 μm and the rectangular shaped cross-section of the coil (a=0 μm, b=100 μm)

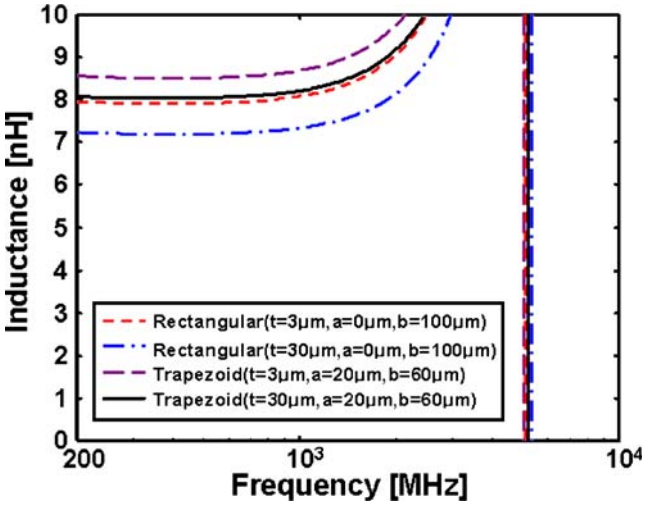

Fig. 4 Simulation results of the *L-f* characteristics with four different Ag/Al_2O_3 inductors with two coil thicknesses (t=3 and 30 μm) and two shapes of cross-section of the coils (*rectangle* with a=0 and b=100 μm and *trapezoid* with a=20 μm and b=60 μm)

the coils under the conditions as Ag/Al_2O_3 structure and t of 30 μm. Here, t of 30 μm was fixed due to its good effect in *Q-f* characteristics shown in Fig. 5. Figure 6 shows the variations of *L-f* characteristics with three different a and b values in trapezoid shaped cross-section of the coils obtained from the computer simulation. As is shown, the L values are nearly constant at 8.1 nH up to 1 GHz, indicating that the change of a and b values will not affect the L values. Figure 7 also shows the variations of *Q-f* characteristics with three different a and b values in trapezoid shaped cross-section of the coils obtained from the computer simulation, illustrating that the highest Q_{max} value of 41 at 700 MHz is observed for the inductors with a=20 μm and b=60 μm. This result is attributed to the same reason mentioned in Fig. 5. The *SRFs* are also constant at 5.2 GHz for all samples as shown in Figs. 6 and 7.

Finally, the simulated *L-f* and *Q-f* characteristics were obtained using various conductivities of the Ag coils under the same conditions as the structure of Ag/Al_2O_3, t of 30 μm, a of 30 μm, and b of 40 μm, are shown in Figs. 8 and 9, repectively. Here, we emphasize that three different conductivities of the Ag coils, such as σ_{Ag} (the bulk conductivity of the Ag material), $\sigma_{Ag}\times 0.7$, and $\sigma_{Ag}\times 0.6$, was considered mainly because the conductivity of Ag lines prepared by direct-write techniques is usually lower than σ_{Ag} [18]. We also chose a of 30 μm although the highest Q_{max} value was observed with a of 20 μm. This is because

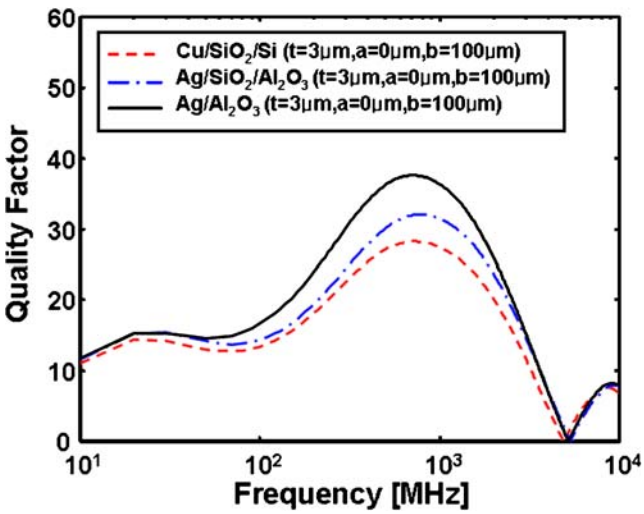

Fig. 3 Simulation results of the *Q-f* characteristics with three structures obtained under the conditions as the coil thickness (t) of 3 μm and the rectangular shaped cross-section of the coil (a=0 μm, b=100 μm)

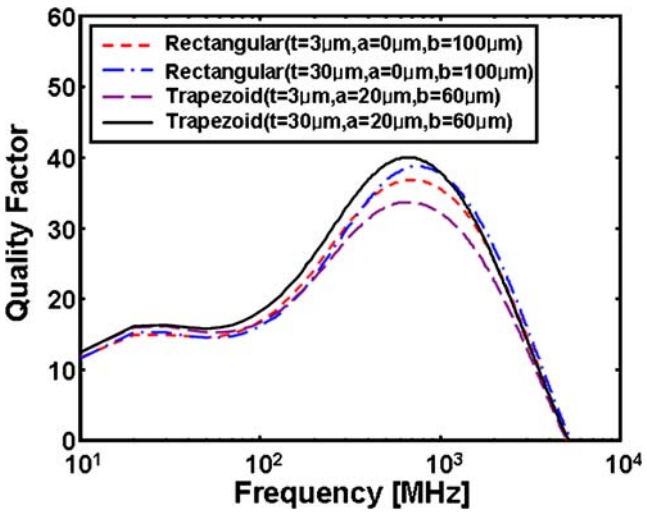

Fig. 5 Simulation results of the *Q-f* characteristics with four different Ag/Al_2O_3 inductors with two coil thicknesses (t=3 and 30 μm) and two shapes of cross-section of the coils (*rectangle* with a=0 and b=100 μm and *trapezoid* with a=20 μm and b=60 μm)

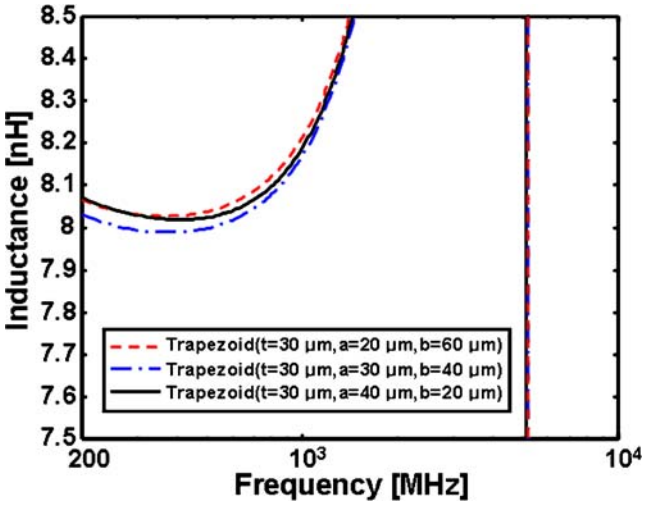

Fig. 6 Variations of *L-f* characteristics with three different *a* and *b* values in trapezoid shaped cross-section of the coils obtained from the computer simulation

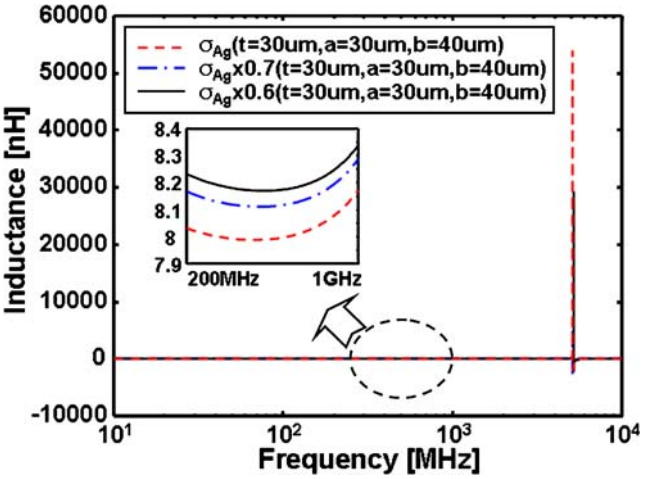

Fig. 8 Simulated *L-f* characteristics obtained using various conductivities of the Ag coils under the same conditions as the structure of Ag/Al_2O_3 , *t* of 30 μm, *a* of 30 μm, and *b* of 40 μm

the Q_{max} value for *a* of 30 μm is slightly lower than that for *a* of 20 μm (see Fig. 7) and *a* of 30 μm is more realistic value when realizing RF micro-inductors prepared by direct-write techniques [18]. It was observed from the inset of Fig. 8 that the *L* values increase slightly as the conductivity of the Ag coils decreases and are nearly constant at 8.2 nH up to 1 GHz for the case of $\sigma_{Ag}\times 0.7$. Figure 9 shows that the highest Q_{max} value is 38 at 700 MHz for the inductors with σ_{Ag}. It was observed from Figs. 8 and 9 that the used inductors with the trapezoid shaped (a=30 μm and b=40 μm) cross-section of the Ag coils, *t* of 30 μm, and the coil conductivity of 70% of Ag bulk value exhibit *L* of 8.2 nH, Q_{max} of 35.5 near 750 MHz, and *SRF* of 5.14 GHz. These results are comparable to those reported in recent literature for various types of MEMS inductors developed using more complex fabrication processes [10–14]. The larger conductivity of the coil, thus smaller resistance of the coil resulted in the larger *Q* effects during high-frequency operation.

Figure 10 shows the well-known equivalent circuit of miniature RF inductors suggested by Ahn and Allen [6] and by Yue and Wong [4]. Here, *R* accounts for the metal resistance that symbolizes the energy loss due to the skin effect in the Ag coils, and *C* represents the stray capacitance due to Al_2O_3 substrates.

In general, the *Q* of an inductor is defined as [1, 2, 4]

$$Q = 2\pi \times \frac{\text{peak magnetic energy} - \text{peak electric energy}}{\text{energy dissipated by the circuit in one period}} \quad (1)$$

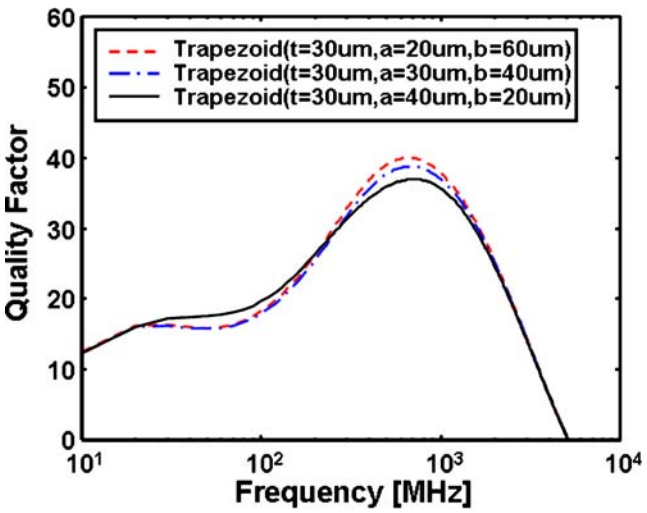

Fig. 7 Variations of *Q-f* characteristics with three different *a* and *b* values in trapezoid shaped cross-section of the coils obtained from the computer simulation

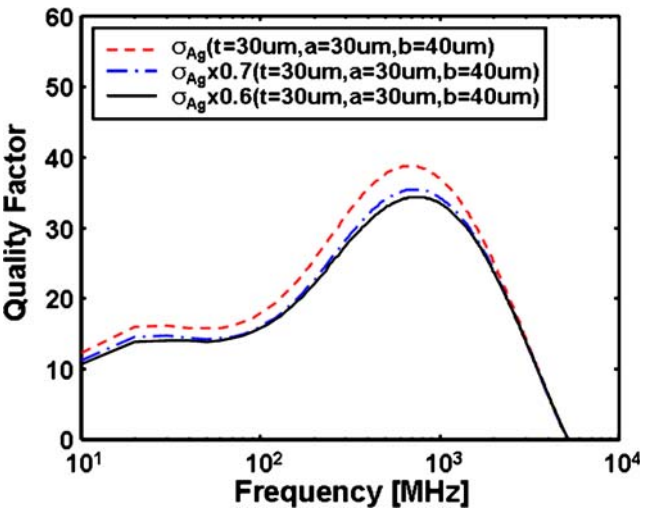

Fig. 9 Simulated *Q-f* characteristics obtained using various conductivities of the Ag coils under the same conditions as the structure of Ag/Al_2O_3 , *t* of 30 μm, *a* of 30 μm, and *b* of 40 μm

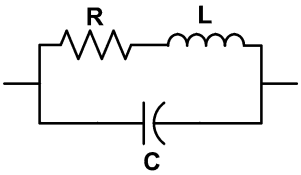

Fig. 10 Equivalent circuit of the RF inductor used to analyze circuit parameters

An inductor is at self-resonance when the peak magnetic and electric energies are equal. Therefore, Q vanishes to zero at SRF [4]. Above *SRF*, no net magnetic energy is available from the inductor to any external circuit. In terms of the equivalent circuit elements in Fig. 10, the magnetic and electric energies can be expressed as:

$$\textit{Peak magnetic energy} = \frac{L}{2} I^2 = \frac{LV^2}{2\left[R^2 + (\omega L)^2\right]}, \tag{2}$$

$$\textit{Peak electric energy} = \frac{C}{2} V^2. \tag{3}$$

The energy loss in one period is the product of the power dissipated by the circuit multiplied by the period $T=2\pi/\omega$. Therefore

$$\textit{Energy loss in one period} = \frac{2\pi}{\omega} \cdot \frac{V^2}{2} \cdot \left[\frac{R}{R^2 + (\omega L)^2}\right] \tag{4}$$

where V denotes the peak voltage across the inductor terminals. The substitution of Eqs. 2, 3, and 4 into Eq. 1 yields the result

$$Q = \frac{\omega L}{R}\left[1 - \frac{R^2 C}{L} - \omega^2 LC\right]$$
$$= \frac{\omega L}{R} \times \text{ self} - \text{resonant factor} \tag{5}$$

where $\omega L/R$ accounts for the stored magnetic energy and the ohmic loss in the resistance. The second term in Eq. 5 is the self-resonant factor describing the reduction in Q due to the increase in the peak electric energy with frequency and the vanishing of Q at the *SRF*.

Figure 11 plots the frequency behavior of Q for the inductors obtained under the conditions as the structure of Ag/Al_2O_3, coil conductivity of σ_{Ag}, t of 30 μm, a of 30 μm, and b of 40 μm. In Fig. 11, the calculated data were obtained from Eq. 5, simulated *L-f* data in Fig. 8, and simulated *C-f* and *R-f* data (not shown). As is shown, the simulated data obtained from a HFSS were found to be in excellent agreement with the calculated data obtained from the equivalent circuit model of the utilized inductors, indicating that the simulated high-frequency data of the inductors and Eq. 5 are very useful for predicting the variation in Q with f of the inductors considered in this work. In Fig. 11, Q is well described by $\omega L/R$ at low frequencies since the self-resonant factor in Eq. 5 is close to unity. As f increases, the self-resonant factor decreases from unity rapidly and thus Q decreases with increasing f.

4 Conclusions

We have successfully computed the high-frequency characteristics of simple, micron size, square spiral-type RF thin film air-core inductors prepared by direct-write supersonic jet deposition of laser ablated silver NP utilizing a HFSS. The area dimensions of RF inductors utilized and the number of coil turns were 1.3 mm×1.3 mm and 3, respectively. The 96 wt% Al_2O_3, SiO_2-coated Al_2O_3, and SiO_2-coated Si wafers were used as the substrate material. Ag lines with the trapezoid shaped cross-section were used as the coils. The Ag/Al_2O_3 was selected as the main structure for simulation mainly because of its simpler structure with the best Q_{max} among all considered structures. It was concluded from the simulated results that either the larger cross-sectional areas of the coil or the larger conductivities of the coil, thus smaller resistance of the coil resulted in the larger Q effects during high-frequency operation and the desired Q_{max} can be achieved by optimizing t, a, and b values. The trapezoid shaped cross-section of the Ag coil and lower conductivities of the Ag coils than σ_{Ag} were considered because they are usual properties for the Ag lines prepared by direct-write techniques. It was also observed that the used inductors with the trapezoid shaped (a=30 μm and b=40 μm) cross-section of the Ag coils, t of 30 μm, and the coil conductivity of 70% of Ag bulk value exhibit L of

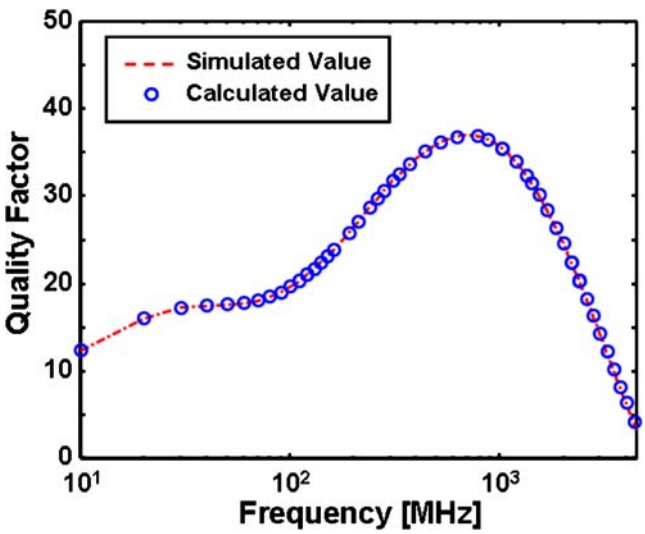

Fig. 11 Frequency behavior of Q for the inductors obtained under the conditions as the structure of Ag/Al_2O_3, coil conductivity of σ_{Ag}, t of 30 μm, a of 30 μm, and b of 40 μm, indicating that the simulated data agree well with the calculated data obtained from Eq. 5

8.2 nH, Q_{max} of 35.5 near 750 MHz, and *SRF* of 5.14 GHz. This was the result comparable to those reported in recent literature for various types of MEMS inductors developed using more complex fabrication processes. It was observed that the calculated data obtained from the equivalent circuit model of the utilized inductors and the derived equation of Q described the simulated high-frequency data of L and Q of the considered inductors quite well.

Acknowledgments This work was supported by the international cooperation programs of the Korea Science and Engineering Foundation (KOSEF) under Grant no. F01-2005-000-10003-0.

References

1. K. Shirakawa, K. Yamaguchi, M. Hirata, T. Yamaoka, F. Takeda, K. Murakami, H. Matsuki, IEEE Trans. Magn. **26**, 2262 (1990)
2. H. Matsuki, N. Fujii, K. Shirakawa, J. Toriu, K. Murakami, IEEE Trans. Magn. **27**, 5438 (1991)
3. R. Groves, D.L. Harame, D. Jadus, IEEE J. Solid-State Circuits **32**, 1455 (1997)
4. C.P. Yue, S.S. Wong, IEEE J. Solid-State Circuits **33**, 743 (1998)
5. J.-B. Yoon, C.-H. Han, E.-S. Yoon, C.-K. Kim, Jpn. J. Appl. Phys. **37**(1), 7081 (1998)
6. C.H. Ahn, M.G. Allen, IEEE Trans. on Industrial Electronics **45**, 866 (1998)
7. T. Tsutaoka, T. Kasagi, K. Hatakeyama, J. Eur. Ceram. Soc. **19**, 1531 (1999)
8. M. Yamaguchi, K. Suezawa, K.I. Arai, Y. Takahashi, S. Kikuchi, Y. Shimada, W.D. Li, S. Tanabe, K. Ito, J. Appl. Phys. **85**, 7919 (1999)
9. S.-G. Kim, E.-J. Yun, J.-Y. Kim, J. Kim, K.-I. Cho, J. Appl. Phys. **90**, 3533 (2001)
10. Y.-K. Yoon, J.-W. Park, M.G. Allen, J. Microelectromechanical Systems **14**, 886 (2005)
11. D.-M. Fang, X.-N. Wang, Y. Zhou, X.-L. Zhao, Microelectron. J. **37**, 948 (2006)
12. C. Lei, Y. Zhou, X.-Y. Gao, W. Ding, Y. Cao, Z.-M. Zhou, H. Choi, Microelectron. J. **37**, 1347 (2006)
13. S.-H. Tseng, Y.-J. Hung, Y.-Z. Juang, M.S.-C. Lu, *Sens. Actuators A: Phys.* **139**(1), 187–193 (2007), DOI 10.1016/j.sna.2006.12.014 (Sept.)
14. A. Mehdaoui, M.B. Pisani, R. Fritschi, P. Ancey, A.M. Ionescu, Microelectr. Eng. **84**(5), 1369–1373 (2007), DOI 10.1016/j.mee.2007.01.222 (May)
15. A. Pique, D.B. Chrisey, Direct-Write Technologies for Rapid Prototyping Applications (Academic, San Diego, 2002), Chapters 1, 4, 6, 17, 18
16. H.C. Kenneth, F. Charlotte, F. Terry, Mat. Res. Soc. Symp. Pro. **624**, 3 (2000)
17. W.T. Nichols, G. Malyavanatham, D.E. Henneke, D.T. O'Brien, M.F. Becker, J.W. Keto, H.D. Glicksman, Appl. Phys. Soc. Lett. Pro. **78**, 1128 (2001)
18. W.T. Nichols, G. Malyavanatham, D.T. O'Brien, D. Kovar, M. F. Becker, J.W. Keto, Mat. Res. Soc. Symp. Pro. **703**, V 5.5.1 (2002)